



<https://doi.org/10.15407/ufm.22.02.175>

A.E. HAFAROV^{1,*}, S.M. VOLOSHKO^{1,},
A. K Aidatzis², and I.A. VLADYMYRSKYI^{1,***}**

¹ Metal Physics Department, National Technical University of Ukraine
'Igor Sikorsky Kyiv Polytechnic Institute',
Prospect Peremohy 37, UA-03056 Kyiv, Ukraine

² Institute of Nanoscience and Nanotechnology, N.C.S.R. Demokritos,
Agia Paraskevi Attikis, 15310 Athens, Greece

* hafarov@kpm.kpi.ua, ** voloshko@kpm.kpi.ua, *** vladymyrskiyi@kpm.kpi.ua

NANOSCALE MATERIALS FOR STATE-OF-THE-ART MAGNETIC MEMORY TECHNOLOGIES

The review deals with different materials science aspects of the state-of-the-art magnetic memory technologies, such as magnetoresistive random-access memory (MRAM), antiferromagnetic (AFM) memory, and skyrmion racetrack memory. Particularly, the materials with high perpendicular magnetic anisotropy (PMA), such as CoFeB, $L1_0$ -ordered Mn- and Fe-based alloys, are considered (Sec. 1) regarding their applications in MRAM technology. Furthermore, studies of AFM alloys, such as FeRh, CuMnAs, Mn_2Au , are reviewed (Sec. 2) with an emphasis on application of these materials in AFM-memory technology. Finally, the last (3rd) section of the review is concerning materials that could be used in skyrmion racetrack memory.

Keywords: MRAM, spintronics, magnetic materials, antiferromagnets, skyrmion.

1. MRAM Materials

1.1. MRAM Technology

Magnetoresistive random-access memory (MRAM) is one of the most promising non-volatile memory approaches because of its low power consumption, fast switching, high endurance, compatibility to modern microelectronics processes, and a high miniaturization potential, as demonstrated by the recently announced 14 nm node [1]. The core component of an MRAM cell is a magnetic trilayer called magnetic tunnel

Citation: A.E. Hafarov, S.M. Voloshko, A. Kaidatzis, and I.A. Vladymyrskiyi, Nanoscale Materials for State-of-the-Art Magnetic Memory Technologies, *Progress in Physics of Metals*, **22**, No. 2: 175–203 (2021)

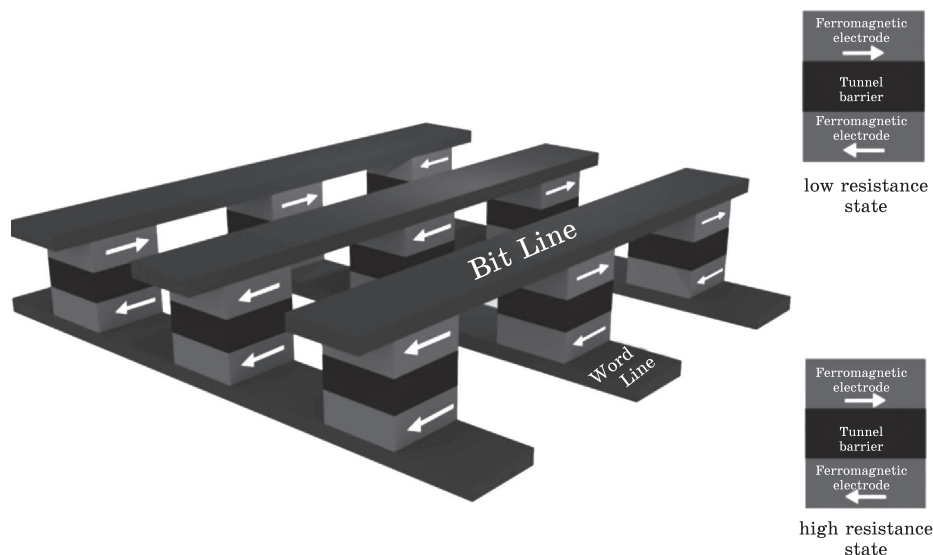


Fig. 1. Simplest representation of MTJ-based MRAM technology. The magnetization of free (top) layer is switched through bit line by spin-transfer torque mechanism

junction (MTJ). In the simplest case, MTJ consists of two ferromagnetic (FM) layers separated by a thin insulating tunnel barrier. The magnetization of the one layer is fixed, while the magnetization of the other layer is free and can be switched between two states — parallel or antiparallel to the fixed layer magnetization. Switching between two magnetization states corresponds to the two different resistance states of the MTJ structure — the states with low and high resistance, corresponding to two states of bit information, respectively. In the mid 1990s, Slonczewski and Berger theoretically predicted that the magnetization direction of a FM layer in multilayer spintronic structures could be switched only by spin-polarized current without application of external magnetic fields. This effect was called spin-transfer torque (STT) [2, 3]. Shortly after, the STT effect was experimentally confirmed and presently STT-MRAM is one of the most promising non-volatile memory technologies. The simplest schematic representation of MRAM architecture is given in Fig. 1.

There are three main requirements for magnetic materials to be successfully used in MTJs. First, FM layers have to provide good bonding with insulator layer (typically, MgO), giving rise to high tunnelling magnetoresistance (TMR). The second requirement is that FM layers have to provide high magnetization thermal stability, a matter addressed by using materials with high magnetic anisotropy energy. The last requirement is the low power consumption of the device, which depends on the low switching current of the FM layers. The critical switching

current of MTJs depends on magnetic Gilbert damping constant (α), and FM materials used in MTJs have to have small damping constant.

At the moment, PMA-CoFeB alloy is the only material that meets all requirements mentioned above. Small lattice mismatch between CoFeB and MgO layers, high interfacial magnetic anisotropy energy and reasonable damping constant of CoFeB made this alloy such successful magnetic material for MRAM applications. However, further increasing MRAM density requires scaling down below the 14 nm node, and CoFeB-based MTJs have reached a limit in miniaturization due to intrinsic materials properties. The reason for this lies in the moderate magnetic anisotropy of CoFeB alloy, which is of interfacial origin. $L1_0$ -ordered Mn-based magnetic materials, such as MnAl or MnGa, seem to be promising option to overcome this limit due to their high magnetocrystalline anisotropy of bulk origin [4, 5]. Both currently used PMA-CoFeB alloys and prospective $L1_0$ -ordered Mn-based alloys are overviewed in the sections following below.

1.2. PMA Cobalt–Iron–Boron Alloys for STT-MRAM Application

Amorphous CoFeB alloy is a currently used magnetic electrode, which shows the highest TMR among all the magnetic tunnel junctions with MgO barrier. CoFe as itself is a magnetic soft alloy and does not reveal high values of magnetocrystalline energy. However, in 2010, Ikeda and co-authors [6] made breakthrough in this direction and found the mechanism of interfacial magnetic anisotropy induced on the boundary between CoFeB and MgO layers for the MTJ stack of complicated Ta/Ru/Ta/Co₂₀Fe₆₀B₂₀/MgO/Co₂₀Fe₆₀B₂₀/Ta/Ru structure [6]. In this case, Ta/Ru/Ta underlayer is intended to improve CoFeB crystallization [7–9], Ta/Ru top layer is introduced to protect MTJs from oxidation, as well as to enhance the magnetic properties of CoFeB layers. As a result, MTJ design with diameter around 40 nm was proven to exist. Moreover, it showed relatively high magnetic-anisotropy energy ($2.1 \cdot 10^6$ erg/cm³) and large TMR. This work allowed advancing CoFeB alloys into MRAM production.

Magnetic anisotropy is a crucial issue regarding MRAM application. Thus, numerous studies are devoted to the investigation of anisotropy energy dependency on different parameters such as thickness of the layers, composition of MTJ stacks *etc.* [6, 10–14]. For instance, it was shown that magnetic anisotropy energy strongly depends on the Ta top layer thickness. SiO₂/Ta/Ru/Ta/Ru/Ta/MgO/CoFeB/Ta(t_{Ta})/[Co/Pd]₆/Ta stacks were deposited by magnetron sputtering (where t_{Ta} denotes the thickness of Ta layer — 0, 0.3, 0.5, and 0.7 nm). It can be clearly seen in Fig. 2 that increase of Ta thickness leads to the significant enhancement of the magnetic anisotropy [15]. This conclusion was confirmed in

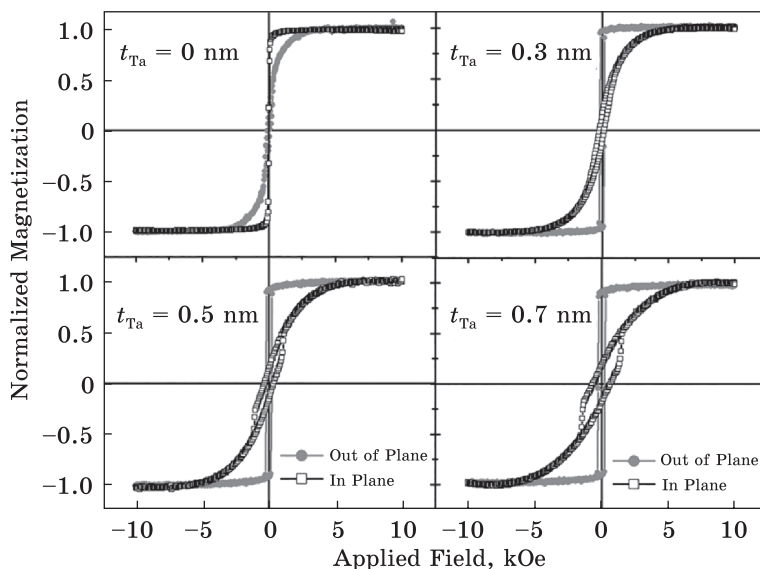


Fig. 2. In-plane and out-of-plane hysteresis loops of CoFeB films with different Ta layer thickness [15]

a number of other studies [16–18]. Moreover, application of Hf layer instead of Ta layer allows increasing the anisotropy energy by 35% [19]. In turn, increase of CoFeB layer thickness [16, 19, 20] as well as increase of MTJ cell lateral size leads to the reduction of the magnetic anisotropy [18]. Despite all these achievements, the issue of relatively low magnetic anisotropy of CoFeB inside MTJs with MgO barrier layer still has not been addressed. It seems that CoFeB reached a limit in the increasing of magnetic anisotropy, meaning that lateral sizes of MTJs cannot be further reduced and memory density cannot be enhanced.

Other key requirement addressed to FM layers of MTJ stacks is a low value of magnetic damping constant. Amorphous CoFeB alloy by itself demonstrates pretty small magnetic damping constant of 0.006, however this parameter significantly increases by a factor of 5 during crystallization [21]. Thus, the lowering of damping constant of crystallized CoFeB layers inside MTJ structures is an important technological issue. There are a lot of approaches that potentially can be used in order to reduce magnetic damping, for example, application of different capping layers [22]. The smallest value of 0.009 was reached for the stack with Cu capping layer. Other study reports that introduction of Al as a capping layer in combination with rapid thermal annealing processing allows to reduce damping constant down to 0.013 [23]. Using of V/Ru and V/Ta as capping layers leads to damping constant reduction as well [24]. Deposition of CoFeB films onto Ru underlayer allows obtaining magnetic damping constant value of 0.007 [25].

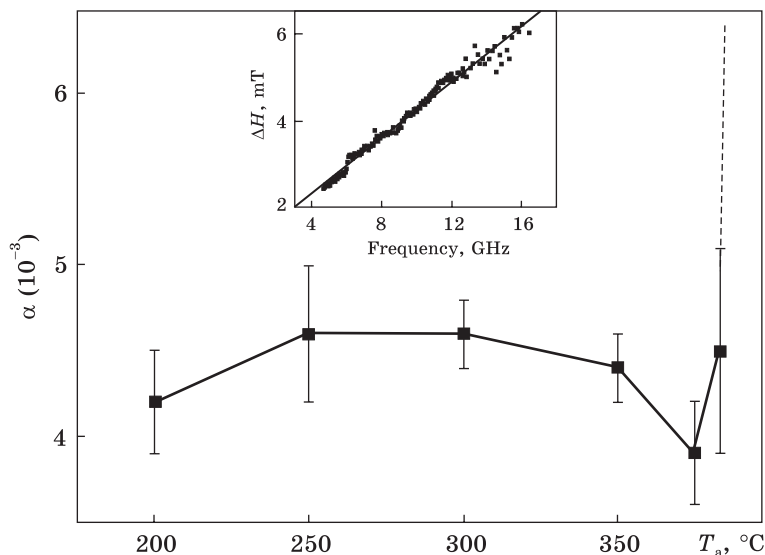


Fig. 3. Effect of annealing temperature on the magnetic damping CoFeB [26]

Conca *et al.* [26] reported that α strongly depends on annealing temperature. $\text{Co}_{40}\text{Fe}_{40}\text{B}_{20}$ films capped with MgO layer were deposited by magnetron sputtering onto SiO_2 substrates with the following heat treatment in vacuum for 30 minutes at different temperatures. Starting from certain temperature (390 °C), magnetic damping constant sharply increases (Fig. 3) [26]. Thickness of CoFeB layer has a significant impact on the magnetic damping as well. For instance, increase of CoFeB layer thickness from 5 nm up to 90 nm leads to reduction of the magnetic damping from 0.009 down to 0.0029 [27].

As a summary, it can be concluded that CoFeB-based MTJs are a very promising option for MRAM spintronic applications due to the high TMR values, relatively high value of magnetic anisotropy energy, and small magnetic damping constant. However, due to the limited magnetic anisotropy of CoFeB further increase of memory density is difficult.

1.3. Manganese-Based $L1_0$ -Ordered Alloys for STT-MRAM Application

MnAl and MnGa alloys are well-known ferromagnets although both of them do not contain any ferromagnetic metal like Fe, Co or Ni. High Curie temperature of 380 °C and moderate saturation magnetization of 600 emu/cm³ were theoretically predicted for MnAl alloys [28]. High values of magnetocrystalline anisotropy energy of up to $15 \cdot 10^6$ erg/cm³ were also achieved experimentally [29–31]. The saturation magnetiza-

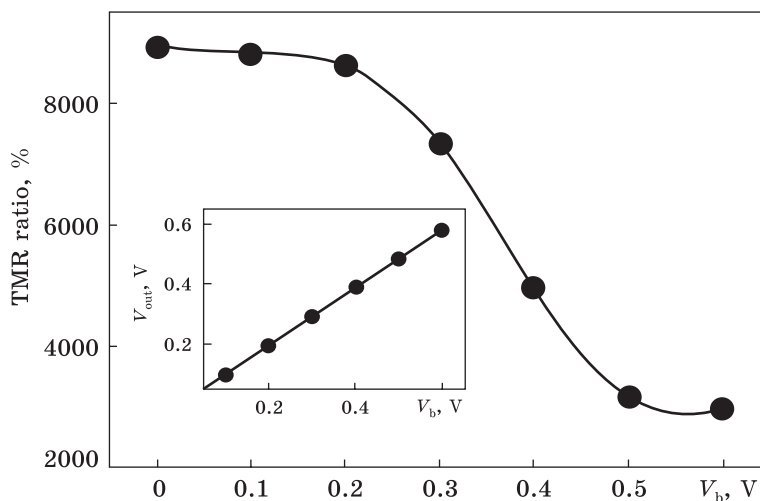


Fig. 4. Results of theoretical TMR calculations for MnAl/MgO-based MTJs [38]

tion of MnAl films can be tuned in a wide range from 40 to 500 emu/cm³ [29, 31, 32]. Similarly to MnAl alloys, MnGa possesses high PMA ($21.7 \cdot 10^6$ erg/cm³) [33, 34] and wide range of saturation magnetization from 27.3 to 270.5 emu/cm³ depending on the film composition and growth conditions [34]. MnGa thin films show ultra-low magnetic damping constant of 0.0003. Even at ultra-low thicknesses MnGa films reveal high magnetocrystalline anisotropy energy of $5 \cdot 10^6$ erg/cm³ [35]. Typically, MnGa films can be deposited on monocrystalline MgO substrates using different underlayers, which make it compatible with MgO-based MTJs [35–37].

Compared to CoFeB, $L1_0$ -ordered hard magnetic alloys offer several advantages for MTJ structures: firstly, strong PMA of MnAl and MnGa films allows designing so-called perpendicular MTJs (p-MTJs) with high thermal stability; secondly, these films on their own have small damping constants. Thus, their use could lead to the reduction of the switching current while keeping high thermal stability. In addition, their moderate saturation magnetization also allows for lowering the required switching current. On the other hand, a problem not solved yet is the low TMR of MTJs based on MnAl and MnGa layers, which is a consequence of the high lattice mismatch between $L1_0$ -MnAl and MgO.

First principles calculations show that theoretically MnAl/MgO MTJs can have extremely large TMR ratio of up to 2000% (Fig. 4) [38]. Experimentally TMR effect of about 2% was observed in MnAl-based MTJs by Saruyama *et al.* [39]. In order to decrease lattice mismatch with insulating layer CoFe underlayer was introduced between MnAl and MgO [39]. Higher TMR ratio of 10% at -268 °C was achieved re-

cently in MnAl MTJs using Co₂MnSi as intermediate layer [40]. Low TMR in this case was explained by presence of defects on the MgO/MnAl interface.

A quite similar behaviour was observed for MnGa alloys. A high TMR ratio of up to 600% was predicted theoretically in Ref. [41]. However, high values of TMR (higher than 100%) have not been experimentally achieved yet. For instance, TMR ratio of 23% at -263 °C was reported for MnGa/MgO/CoFe MTJs [41].

The reason why MTJs that contain MnAl or MnGa as FM layers and MgO as insulating layer do not show high TMR ratio is the large lattice mismatch between FM layer and MgO (higher than 7%) [29, 42]. The L1₀-MnAl phase has lattice constants of $a = 0.394$ nm and $c = 0.356$ nm [29]. The L1₀-phase of MnGa has lattice constants of $a = 0.388$ nm and $c = 0.364$ nm [42]. At the same time, MgO has lattice parameter $a = 0.4212$ nm. The use of intermediate layers between FM and insulating layers is intended to reduce lattice mismatch thereby increasing TMR of MTJs. There are a lot of different magnetic and non-magnetic layers that can be used in MnAl- or MnGa-based MTJs such as Cr, CrRu, CoFe, Co₂MnSi, CoGa, CoFe *etc.* [29, 40, 41, 43, 44]. For example, introduction of Co₂MnSi between the MnGa and MgO layers was reported by S. Mao and TMR of 40% at -263 °C was achieved in the MnGa/Co₂MnSi/MgO/Co₂MnSi/MnGa MTJs. Both the top and bottom MnGa electrodes show a pronounced PMA and a strong antiferromagnetic coupling in the MnGa/Co₂MnSi bilayer [40]. A relatively high TMR ratio of 27% was achieved in MnGa(25 nm)/Co(0.8 nm)/MgO(2.3 nm)/Fe(5 nm)/Pd(2 nm) p-MTJ stacks grown by molecular beam epitaxy on GaAs substrates [38]. A thin Co layer was used to improve the interface quality between the MnGa and MgO and to reduce the lattice mismatch. A strong antiferromagnetic coupling was observed between the MnGa and Co layers. MnGa MTJs in combination with CoFeB layer show TMR ratio of up to 40% at room temperature (RT) [42, 43]. Introduction of an additional layer outside of MTJ to form a strained MnGa layer with an increased lattice parameter is another possible route to reduce lattice mismatch [42].

So far, there has not been any report about a high TMR value for MnAl-based MTJs. Recently several investigations were performed regarding MgO/MnAl thin films. It seems that introduction of different intermediate layers not only allows to reduce lattice mismatch but also to tune other magnetic properties like magnetization, anisotropy energy or coercivity. For instance, introduction of Cr₁₀Ru₉₀ buffer layer allows to achieve a moderate value of M_s (500 emu/cm³) and a surface roughness of the MnAl film of about 0.34 nm while keeping a high value of K_u ($13 \cdot 10^6$ erg/cm³) [45]. Introduction of Cr or CrRu intermediate layers is a promising way to reduce lattice mismatch between MnAl and MgO layers [29, 45, 46]. However, the impact on the TMR performance

is yet to be investigated. It has been shown that Co substitution into the MnAl layer is an effective approach to reduce the saturation magnetization (from 560 to 350 emu/cm³) and surface roughness down to 0.2 nm [46]. The roughness of FM layers is another important parameter for design of effective MTJ elements: lowering of the roughness leads to less destruction of the MTJ structure.

Application of FM materials as an intermediate layer is another promising approach to increase TMR. Using two FM layers, one of which has strong PMA and the second one improves bonding with the MgO barrier, could allow achieving high TMR, high thermal stability and low power consumption [47]. One of the benefits of such layer stack is that two FM layers in MTJs could be exchange coupled (ferromagnetic or antiferromagnetic coupling) forming a so-called synthetic antiferromagnet. Switching of one layer could lead to the switching of the second one. This approach was tested on $L1_0$ -ordered MnGa-based MTJs. For example, MnGa/Co exchange coupled systems were investigated, and MnGa/Co/MgO/CoFeB MTJs with TMR of about 40% at RT has been demonstrated [43].

Very recently, Suzuki *et al.* realized ultrathin MnGa layer (1 nm) in combination with CoGa layer (30 nm) and applied it as a free layer in the MTJ structure. CoFeB was used as an electrode with fixed magnetization. The MnGa/MgO interface was modified by adding several monolayers of Mn in order to increase the TMR ratio. The samples with inserted Mn layers reveal an increased TMR ratio compared to the reference samples without the Mn (TMR increase from 1.7 to 19%). Furthermore, the samples do not show an increase of the M_s . It was observed that MnGa and Mn demonstrate ferromagnetic coupling at the interface [48]. Because of the large bulk magnetic anisotropy of the bottom FM layer, such systems can be a promising solution for further downscaling of MTJ cells below 14 nm.

Mn-based $L1_0$ -alloys are of a great interest for MRAM spintronic application because of their promising magnetic properties such as high bulk magnetic anisotropy energy, high tunability of saturation magnetization and low magnetic damping constant.

High magnetocrystalline anisotropy of MnAl and MnGa thin films allows designing very small MTJ elements (diameter of less than 20 nm) thereby sufficiently increasing memory density. However, there is a limitation in the form of low TMR of MnAl- and MnGa-based MTJs, that appears due to big lattice mismatch with MgO layer. Some material science approaches such as introduction of additional layers, inducing of external stresses, optimization of heat treatment parameters, *etc.* seem to be prospective for achieving high TMR ratio in these types of MTJs. Mn-based MTJs of high TMR could result in the replacement of CoFeB from MRAMs manufacturing.

1.4. Iron-Based $L1_0$ -Ordered Alloys for MTJ-MRAM Application

$L1_0$ -ordered FePt alloys are well known for years as main material for high-density HDD memory because of high values of magnetocrystalline anisotropy and coercivity. However, investigations of FePt alloys are not limited in HDD memory direction, and a lot of investigations are related to MTJ-MRAM application.

Inami *et al.* have been investigated magnetic properties of perpendicularly magnetized MTJ stack of Ta/CoPt/MgO/FePt/Pt/Cr/MgO [49]. In order to obtain the ordered $L1_0$ structure with perpendicular magnetization, CoPt and FePt layers were sputtered at 675 K and 775 K, respectively. The thinnest FePt layer, which reveals PMA, was found to be 4 nm thick. A clear switching between parallel and antiparallel magnetization of FM layers was found in the field of ≈ 2 kOe. However, rather low TMR ratio of about 6% was obtained at room temperature. Yang *et al.* prepared perpendicular MTJs stacks of FePt(5 nm)/MgO(3 nm)/FePt(20 nm) by molecular beam epitaxy and received TMR ratio of 21% and 53% at 300 K and 10 K, respectively [50].

Despite the fact that $L1_0$ -FePt nanoscale structures have great PMA and possibly could be very promising choice for MTJs electrodes, however, high enough TMR ratio were not achieved for FePt-based MTJs. Moreover, high values of magnetic damping constant do not allow to successfully using them in real MRAM devices.

On the other hand, $L1_0$ -ordered FePd alloy is other promising Fe-based ferromagnetic material that can be used as MTJ electrode. Last couple of years, FePd MTJs are intensively studied. Similar to FePt alloys, tetragonal $L1_0$ -FePd phase can be obtained *via* heat treatment and transition from A1 cubic phase. Experimentally was shown high values of magnetocrystalline energy of $K_u \approx 1.3-1.4 \cdot 10^7$ erg/cm³ and low values of damping constant of $\alpha \approx 0.002$ [51–53] for $L1_0$ -FePd, which make it a very prospective candidate in MTJ-MRAM application. The main problem with using of FePd as MTJ electrode is that the A1– $L1_0$ transition temperature is about 500 °C, which leads to undesirable diffusion processes in MTJ, such as penetration of Pd into other layers. One of the approaches to deal with it is reducing of transition temperature by introduction of additional layers to the FePd. For instance, introduction of thin Co₂MnSi layer lead to decrease of transition temperature to 400 °C [54]. Ru seed layer is the other option for using FePd in MTJs [55]. The other way is introduction of diffusion barrier layers. Zhang *et al.* fabricated combined FePd and CoFeB-based MTJ stacks with and without additional diffusion barrier layers of Ta/W between CoFeB and FePd. Compared to the FePd p-MTJs without the diffusion barrier (almost ‘zero’ TMR), stacks with Ta and W diffusion barriers reveal 8.0% and 7.0% RT TMR ratios, respectively [56].

Although high values of TMR were not achieved for FePd-based MTJs, still FePd remain a very prospective material for future application in MTJ production. Most likely in the nearest years, a lot of investigations regarding $L1_0$ -FePd MTJs will be done.

2. Antiferromagnetic Memory Materials

2.1. AFM Memory Technology

Commonly, magnetic memory industry uses ferromagnets (FM) as a main storage material. The main reason for this being the fact that ferromagnetic order can be easily detected by the magnetic field it creates. In addition, it can be easily manipulated by a weak external magnetic field. In contrast, antiferromagnetic materials (AFM) are almost indifferent to external magnetic fields (except very large ones) and cannot be manipulated by them. However theoretically, AFMs can be used as materials for memory application, just like FMs. In this regard AFM materials have a couple of undeniable advantages compared to FM. (i) Typically AFM states can be manipulated much faster compared to FMs (picoseconds *vs.* nanoseconds, respectively. (ii) AFMs are much more stable at magnetic fields. (iii) Materials such as CuMnAs or Mn_2Au reveal high Néel temperature (more than 450 K [57, 58]), allowing the enhancement of working temperatures of spintronic devices. The main issues related to application of AFMs in spintronics are detection and control of their magnetic states. Fortunately, new effective approaches for manipulation of magnetic states in FMs were discovered, *e.g.*, by electrical current (realization of spin transfer torque (STT) effect in MTJs), which promoted the interest for investigation of AFM as well. In particular, the utilization of electrical currents instead of magnetic fields renewed interest in AFM regarding memory applications. For instance, AFM memory was recently realized using FeRh films grown on MgO(001) substrates [59, 60]. In this regard, FeRh reveals first-order magnetic phase transition from AFM to FM states at ≈ 90 – 100 °C [59, 61]. The main idea of AFM memory based on FeRh alloy lies in the distribution of magnetic domains in different directions, that is obtained after the application of magnetic field to the film during cooling from 127 °C (FM phase) to 27 °C (AFM state). Such distribution allows obtaining high- and low-resistance states, which in turn allows using of this material as typical memory cell. This report was the first indication that a single AFM material can be successfully used as memory medium and first push for development of AFM spintronics [59, 62]. Furthermore, AFM can work in terahertz mode showing ultrafast spin excitations, which means that memory device made from such a material could allow to read/write information much faster than any FM-based device [63, 64]. But still, the whole process of information processing

using FeRh alloys requires application of both heating and magnetic field, which complicates the practical use of these materials. Thus, investigation of FeRh and similar phases that reveal AFM–FM transition is vital issue in modern spintronic branch.

In 2016, Wadley *et al.* [65] reported electrical switching of magnetization in tetragonal AFM semiconductor CuMnAs *via* Néel spin–orbit torque switching. Meanwhile, the current density needed for switching of spin axes is $4 \cdot 10^6 \text{ A} \cdot \text{cm}^{-2}$ which is much smaller than in FM [65]. Later such phenomenon was demonstrated for Mn₂Au films revealing switching current density of $\sim 10^7 \text{ A} \cdot \text{cm}^{-2}$ [66]. These studies again gave a powerful impetus to the AFM spintronic investigations, since now memory cell could be created based on thin AFM layers. Moreover, their magnetic states can be easily manipulated without using any magnetic fields or heating.

Other promising approach for AFM memory deals with piezoelectric strain-controlled AFM memory and was demonstrated by Han Yan *et al.* in 2019. MnPt thin films were sputtered onto piezoelectric 0.72PbMg_{1/3}Nb_{2/3}O₃–0.28PbTiO₃ (PMN–PT) single-crystal substrates. As a result, a non-volatile electrical resistance modulation in a high-Néel-temperature intermetallic compound *via* piezoelectric strain was achieved. The tunneling anisotropic magnetoresistance of $\approx 11.2\%$ at RT was reported. Significant advantage of this approach lies in the fact that writing and reading realized in such memory devices are robust under high magnetic fields due to the absence of any other magnetic materials except AFMs [67].

Thus, for now, AFM spintronics attract high interest among scientists and investigators. However, there are a lot of technological hurdles that have to be surpassed for successful application of these materials in spintronic memory production. Most of these are related to material science issues. For the most cases, high quality, excellent (001) epitaxy and high stability at low thicknesses are required for films preparation. All of these can be satisfied by applying typical material science approaches like varying of substrate type, deposition parameters, additional treatments, *etc.* At the moment, FeRh thin films with AFM–FM transition as well as CuMnAs and Mn₂Au thin films that demonstrate the possibility of electrical current switching are the most promising materials for future application in AFM memory. Thus, below we will focus on material science review of these alloys.

2.2. Structural and Magnetic Properties of Promising AFM Materials

2.2.1. Iron–Rhodium Alloy for AFM-Memory Application

FeRh is a chemically ordered alloy with a B2 (CsCl) structure showing first order magnetic transition from the AFM (α'') to FM (α') states at a temperature range between 27 °C and 97 °C upon heating from RT. This

phase transition is accompanied by an isotropic volume expansion of about 1% and sufficient reduction in the resistivity [61]. The α'' phase crystal lattice consists of Fe atoms antiferromagnetically ordered in the (001) direction (net magnetic moment of $3.3\mu_B$) and Rh atoms with zero net magnetic moment. In contrast, α' phase provides ferromagnetic order of all atoms with Fe net magnetic moment of $3.2\mu_B$ and Rh net magnetic moment of $0.9\mu_B$ [61]. The bulk lattice parameters of α'' -FeRh and α' -FeRh phases are 2.985 Å and 2.995 Å, respectively [68].

For practical applications, phase transition temperature has to be sufficiently higher than RT in order to be stable at RT. On the other hand, phase transition temperature is not supposed to be high enough to cause any undesired effects, like phase transitions or diffusion processes during reading/writing processes. Thus, control over transition temperature in FeRh films is a crucial issue. It was shown that AFM–FM phase transition temperature, as well as stability of FM state, depends on the thickness of the film. Thin films with different thicknesses of the ordered FeRh alloy were obtained on MgO(001) substrates at 530 °C by ultrahigh vacuum magnetron sputtering. The thicknesses of the films were varied from 10 to 160 nm. Annealing at 800 °C in vacuum for 1 hour was applied in order to promote the ordering of atomic structure. Results showed that films with a thickness of 10 nm reveal smaller temperature of phase transition (RT) compared to 20 nm thick films (≈ 110 °C). Thicker films demonstrate magnetic behaviour similar to 20 nm thick films [69]. It seems that stresses occurring at the interface between film and MgO substrate play the key role in temperature–thickness dependence. Most of the studies related to FeRh films are investigating well-textured (001)-films grown on MgO(001) substrates. However recently, it was observed that crystallography has significant impact on the phase transition in this alloy. 90 nm thick equi-atomic FeRh thin films were magnetron sputtered-deposited at 525 °C onto different single crystal substrates of different epitaxial orientations — MgO(001), MgO(111), and *c*-Al₂O₃(0001). Right after the deposition, films were heat treated in vacuum at 700 °C. It was reported that the in-plane strain changes from compressive type in case of MgO(001) to tensile one using *c*-Al₂O₃(0001), affecting the magnetic properties of the films. The tensile stress of FeRh films on the sapphire substrate leads to decrease the AFM–FM transition temperature due to larger cell size, promoting stabilization of the FM phase at lower temperatures [61].

The connection between variation of the film thickness and changes in the temperature of phase transition in the wide range (200 °C) was proven in Ref. [68]. FeRh films with thicknesses of 10, 15, 22, and 100 nm were deposited onto three different substrates (MgO, KTaO₃ (KTO), and SrTiO₃ (STO)) at 600 °C. The measurements of phase transition tem-

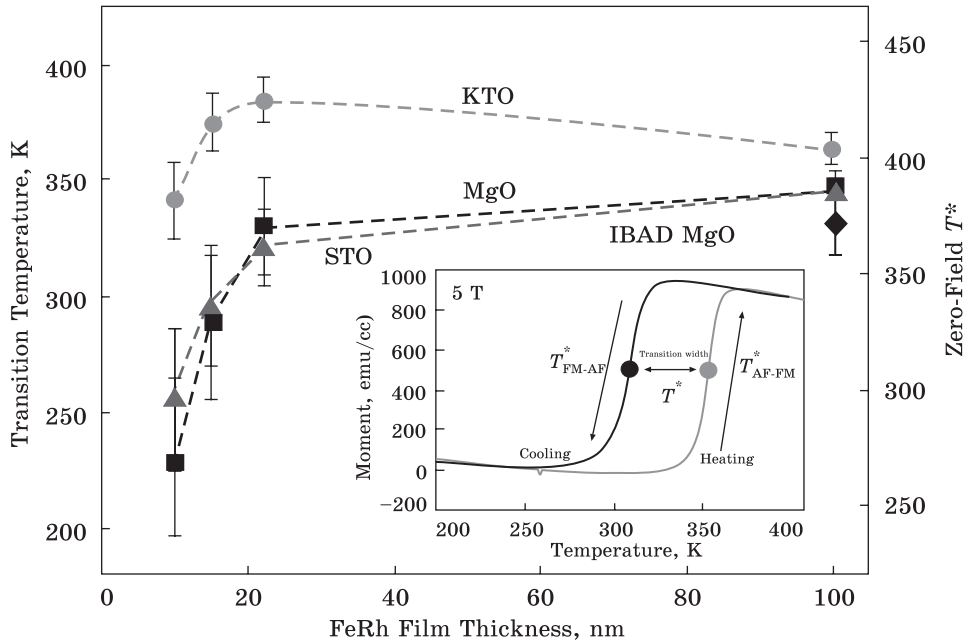


Fig. 5. Dependence of the transition temperature on the film thickness [68]

perature indicate clear dependence on the film thickness and type of the substrate, as shown in Fig. 5. Application of KTO substrate allows increasing transition temperature up to 75 °C even at relatively small thicknesses of the film. A key factor that defines transition temperature is the appearance of the strains at the film/substrate interface. Tensile strains induce decrease of the transition temperature, in turn compressive strains lead to the temperature increase. In this case, KTO substrates produce sufficient compressive strain for the rise of transition temperature above RT in 10 nm thick FeRh films [68].

FeRh can also be used for coercivity tuning of other magnetic thin films. For example, coercivity of Ni films deposited on FeRh layer can be varied by tuning of deposition conditions. $\text{Fe}_{50}\text{Rh}_{50}$ films were grown on MgO(001) substrate at 300 °C using DC magnetron sputtering and subjected to the following post annealing at 800 °C in vacuum. After that, 15 nm thick Ni layer was deposited onto FeRh film at two different temperatures: RT (below temperature of phase transition) and 250 °C (above temperature of phase transition). As reported, the coercivity of Ni film deposited at high temperature with cooling to RT afterwards increases by 500% compared to Ni films deposited initially at RT. The weakly textured Ni film creates inhomogeneous strain gradients along grain boundaries of different orientations, allowing pinning domain walls and leading to enhancement of the coercivity [71].

Thus, currently FeRh films demonstrate great potential for AFM memory devices. Due to the unusual FM–AFM phase transition during cooling, FeRh can provide two stable states with high and low resistivity, which can be used as bits of stored information. The transition temperature is crucial parameter for such application and it depends on many intrinsic and extrinsic factors. The properties of FeRh alloy can be successfully tuned over wide ranges varying different substrates, thicknesses of FeRh layer, alloying by additional magnetic and non-magnetic elements, changing deposition parameters. Stresses induced in FeRh films play a key role in AFM–FM transition. Thus, any external influence that causes appearance of additional stresses in FeRh layer provides significant effect on the transition temperature.

FeRh thin films were intensively investigated in the last couple of years, and there are still a lot of material science issues that have to be solved, *e.g.*, optimization of deposition conditions, choice of the appropriate external treatments, *etc.* FeRh AFM memory devices could be implemented in manufacturing in the nearest future based on the current state-of-the-art. The only disadvantage of this technology is that magnetic field has to be applied during writing. Nevertheless, despite this limitation, FeRh-based AFM memory still is one of the most promising technologies for future non-volatile memory applications.

2.2.2. Copper–Manganese–Arsenic Alloy for AFM-Memory Application

Despite the fact that bulk CuMnAs alloy has orthorhombic crystal structure, nanoscale CuMnAs thin films could be grown with tetragonal crystal lattice (Fig. 6). Lattice parameters of tetragonal structure are $a = b = 3.820 \text{ \AA}$, $c = 6.318 \text{ \AA}$ [72] and Néel temperature is approximately $210 \text{ }^\circ\text{C}$ [65, 73]. Antiferromagnetism in CuMnAs alloys was theoretically predicted and experimentally proved in 2012 [74]. Later the epitaxial growth of tetragonal AFM CuMnAs thin films by molecular beam epitaxy on both GaAs and GaP substrates was shown, proving that CuMnAs is compatible with existing semiconductor technologies [72]. Moreover, electrical current switching mechanism in the GaAs/CuMnAs films was shown experimentally, and it was concluded that switching mechanism is dominated by thermal activation [75]. Low energy switching *via* nanosecond current pulses was later demonstrated for the CuMnAs films on GaP (100) substrate [73]. CuMnAs layer with thickness of 46 nm was grown using molecular beam epitaxy onto 100 nm GaP underlayer. Orthogonal switching in the films with single 25 mA current pulse with pulse width of 4 ns [73].

CuMnAs is one of the promising candidate materials for AFM memory application. The fact that it is possible to switch magnetic order with electrical current is its main advantage compared to FeRh. However, a great deal of materials investigation is yet to be done for CuMnAs.

2.2.3. Manganese–Gold Alloy for AFM-Memory Application

Another promising candidate for application in AFM spintronics is Mn_2Au alloy. Mn_2Au possesses a body-centred tetragonal crystal lattice, which can be used as tetragonal free layer with strong PMA [77]. Lattice parameters of Mn_2Au are $a = 3.328 \text{ \AA}$ and $c = 8.539 \text{ \AA}$ [78]. First-principles calculations reveal very high Néel temperature of $1230 \text{ }^\circ\text{C}$ for this material [79].

Neutron diffraction study gives a clear picture of magnetic moments directions inside Mn_2Au lattice as shown in Fig. 7. The orientations of Mn moments from ferromagnetic layers perpendicular to c axis alternate from one layer to another [80].

Mn_2Au thin films can be grown on Al_2O_3 ($1\bar{1}02$) substrate [81, 82], and typically there is no clear epitaxy along c -axis in that case due to alumina crystal structure. However, Mn_2Au can be epitaxially grown on Al_2O_3 substrate using Ta(001) as a buffer layer [83]. Another option for strict epitaxial growth of Mn_2Au films is MgO(001). For example, MgO/ZrN/ Mn_2Au /ZrN stack reveals great epitaxy [78]. ZrN buffer layer being used for reduction of mismatch between MgO and Mn_2Au (from 11% to 3%). The Mn_2Au layer was deposited by dc magnetron sputtering and ZrN layer was obtained by reactive sputtering in an Ar/N mixture at different substrate temperatures [78]. X-ray diffraction studies indicated that Mn_2Au crystal orientation strongly depends on the substrate temperature during deposition. It seems that heating of the substrate up to $450 \text{ }^\circ\text{C}$ allows to obtain excellent (001) epitaxy (Fig. 8) [78].

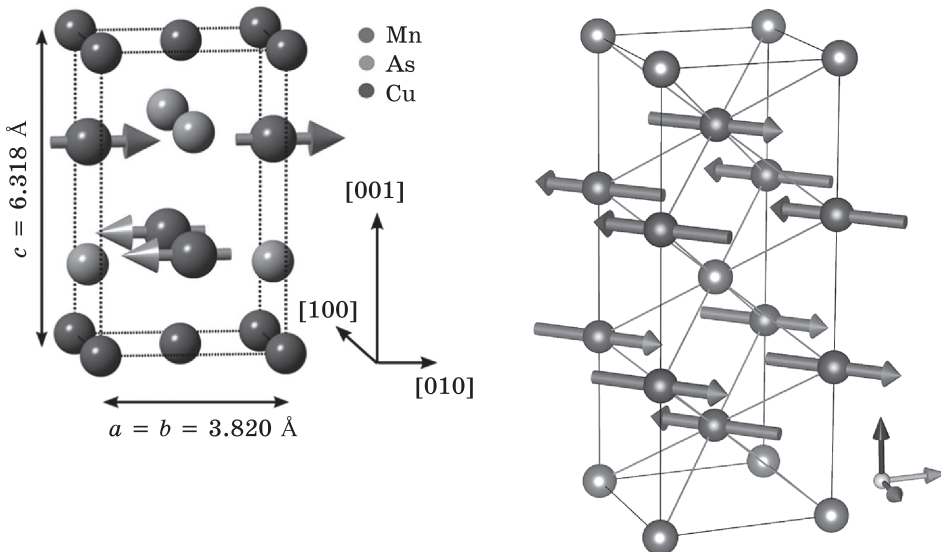


Fig. 6. Tetragonal CuMnAs lattice representation [76]

Fig. 7. Magnetic structure of Mn_2Au derived from the neutron diffraction study [80]

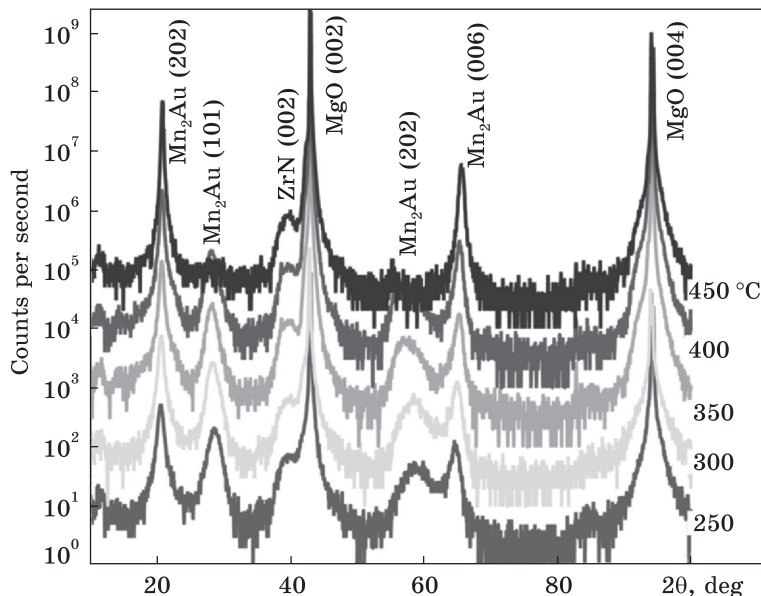


Fig. 8. X-ray diffraction patterns of MgO/ZrN/Mn₂Au/ZrN stacks deposited at different substrate temperatures (from 250 to 450 °C) [78]

Similar to CuMnAs, Mn₂Au alloy is also a potential candidate for non-volatile memory applications as it allows for electrical current switching, although further materials development is required.

3. Skyrmion Memory

3.1. Skyrmion Memory Technology

Skyrmion racetrack memory is another promising technology that can be implemented in the nearest future as ultra-dense, low-cost and low-power storage technology [84, 85]. Skyrmions are swirling spin textures that occur in magnetic material under certain circumstances (Fig. 3). Inside the skyrmion, spins gradually change their directions to antiparallel from the centre of the skyrmion to its edge. Generally, spin configuration inside skyrmion is defined by interfacial or bulk Dzyaloshinskii–Moriya interaction (DMI). Typically, interfacial DMI arise from FM/heavy metal interface [86–88] and bulk DMI — in non-centrosymmetric crystals [89–91]. Depending on the nucleation conditions (crystal structure, substrate, *etc.*), skyrmions of two types can be created: Bloch-type (Fig. 9, *a*) and Néel-type (Fig. 9, *b*) skyrmions [92], defining what kind of spins unrolling will be present inside skyrmion. Initially skyrmion-type structures were observed in bulk helical MnSi and CoFeSi magnets [90, 93]. Later, skyrmions existence was proven in CoFeSi thin

Fig. 9. Visual representation of Néel-type (a) and Bloch-type (b) skyrmions [92]

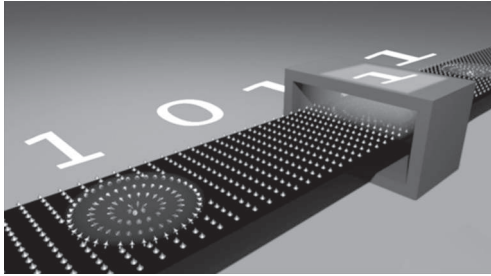
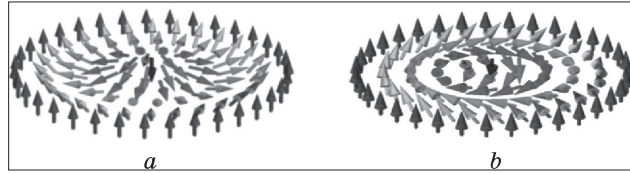


Fig. 10. Schematic view of skyrmion racetrack memory

films [94] as well as in Fe monolayers and PdFe bilayers on Ir(111) [95, 96]. The main issues in past was related to the difficulties of single (not skyrmion lattice or spin spirals) skyrmion creation and skyrmion stabilization. High magnetic fields (higher than 1 T) and low temperatures ($-243\text{ }^{\circ}\text{C}$) were needed for skyrmion stabilization, which prevented any practical application. Recently, numerous groups demonstrated stabilization of skyrmions at lower magnetic fields and at room temperature [97–99].

The concept of skyrmion memory is based on the fact that skyrmions can be nucleated and then move along thin material. Thus, racetrack-type memory device can be designed using skyrmions: by creating and moving of skyrmions in certain areas of thin ribbons, some bit sequence can be written (Fig. 10).

In order to design a memory device, one needs to manipulate skyrmions: specifically create, destroy and move them along material. There are several known ways to manipulate skyrmions, but only two of them are of the greatest practical interest: control by spin-polarized currents and control by external electrical field. In the first case, locally applied spin-polarized electrons with several hundreds of nanoamps and the applied bias voltage to several hundreds of millivolts are enough to create and destroy single skyrmion, which can be easily interpreted as writing/deleting of one bit. This effect was firstly shown in Ref. [95]. The second method does not require spin-polarized electrons and allows controlling skyrmions by local electric-field effects combined with an electrical detection method. The basis of this approach is so-called non-collinear magnetoresistance (NCMR) effect and it allows manipulating skyrmions with non-magnetic electrodes [100–102]. Moreover, skyrmions can be moved along material using STT mechanism [95, 103–107].

Thus, skyrmion spintronics seems to be a very promising approach for novel memory applications, due to its possible high density, low energy consumption and low cost. At the moment, two main groups of materials are mostly investigated regarding skyrmion memory application: (i) ultrathin epitaxial films and multilayers, which typically contain several monolayers of Fe or Pd on Ir(111) underlayer [108–110]; (ii) sputtered multilayers (*e.g.*, (Pt/CoFeB/MgO(1.4))₁₅, (Pt/Co/Ta)₁₅, (Ir/Co/Pt)₁₀ [111–123]). In the first group, skyrmions are typically very thin (couple of nanometres), but at the same time are unstable at RT and low magnetic fields. Although their limited size is a good feature for ultra-high density memory, if they cannot be stabilized at RT, it is not possible to be used in manufacturing. Increase of the thickness as well as increase of the amount of interfaces using multilayer structures seems to be an effective route to stabilize skyrmions at RT without the use of high magnetic fields. Thus, the second group of materials is more reliable in this regard. Despite the larger size of skyrmions (more than 40 nm), multilayers provide higher potential for practical use. The actual issue of modern skyrmion spintronics is the creation and stabilization of a single small skyrmion at RT with low energy consumption. The quality, size, mobility and any other important parameters of skyrmions are strongly dependent on crystal structure of magnetic material, type of the substrate, methods of obtaining, and type of defects presented in material. Thus, further we will focus on material science issues of skyrmion spintronics. Mostly, multilayer stacks will be discussed, since they are of most practical interest.

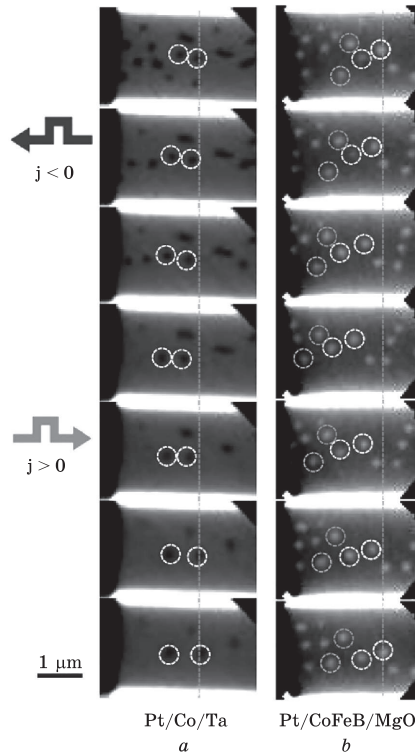
3.2. Cobalt–Iron–Boron-Based Skyrmions

CoFeB thin layers are supposed to be promising materials for skyrmion application due to the high interfacial DMI of CoFeB layers bonded with heavy metal layers with strong spin–orbit coupling (SOC). For instance, it was shown that Pt(2 nm)/Co₄₀Fe₄₀B₂₀(0.8 nm) stacks demonstrate high DMI constant of 1.0 mJ/m² [111]. Films were deposited onto thermally oxidized Si substrate by magnetron sputtering at RT with the following heat treatment at 240 °C for 1 hour. The use of thin CoFeB layer of approximate 3 atomic planes thickness in combination with Pt layer allows inducing high interfacial DMI. As mentioned before, strong DMI is the main driving force for skyrmion nucleation. Later, experimental existence of skyrmion lattice at RT as well as movement of separate skyrmions *via* short current pulses were demonstrated in (Pt(3 nm)/CoFeB(0.7 nm)/MgO(1 nm))₁₅ stacks [108]. CoFeB was used in amorphous state in order to decrease skyrmion pinning due to the absence of grain boundaries. Compared to polycrystalline Pt/Co/Ta films, skyrmion reveals higher velocity of movement (46 ms⁻¹ *vs.* 30 ms⁻¹). Moreover, movement

Fig. 11. Skyrmion movement in Pt/Co/Ta (a) and Pt/CoFeB/MgO (b) thin films [108]

of skyrmions in amorphous CoFeB is not accompanied by their destruction (Fig. 11).

W layer can be used as heavy metal in combination with CoFeB, similarly to Pt. High DMI constant of 0.73 mJ/m^2 at RT of sputtered W(5 nm)/Co₂₀Fe₆₀B₂₀(0.6 nm)/MgO(2 nm) thin films was achieved by Jaiswal *et al.* [112]. It was shown that change of CoFeB chemical composition strongly affects the DMI strength. For instance, Co₄₀Fe₄₀B₂₀ films demonstrate DMI constant of 0.28 mJ/m^2 . The deposition conditions also have a great effect on the domain structure, increase of sputtering power (from 400 W up to 1500 W) allows to sufficiently smoothing domains, which directly affect the skyrmion pinning during movement.



On the example of stack with Ta as heavy metal layer in combination with Co₂₀Fe₄₀B₂₀(0.8 nm), it was shown that DMI constant strongly depends on the annealing temperature (Fig. 12). Although DMI constant

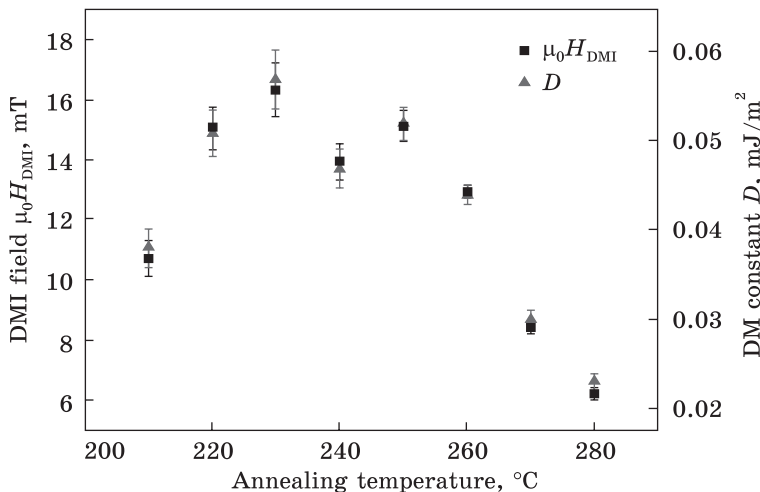


Fig. 12. DMI constant dependence on the annealing temperature (pink triangles) [113]

does not reveal high values, this work clearly indicates that obtaining and treatment parameters define the character of magnetic interaction, directly influencing the skyrmion properties [113].

Qin *et al.* [114] showed that the size of skyrmions could be controlled by varying the thickness of Ta layer. $(\text{Ta}(t_{\text{Ta}})/\text{CoFeB}(1.1 \text{ nm})/\text{MgO}(1.0 \text{ nm}))_{15}/\text{Ta}(2 \text{ nm})$ films were deposited using magnetron sputtering; thickness of Ta layer was varied as 1.0, 1.8, 2.5 and 5.0 nm. Increasing the thickness of Ta layer led to increase of the skyrmion size as well (from 150 nm up to 300 nm). Reversal of sputtering order in Ta/CoFeB stacks affected the CoFeB crystalline structure and amount of defects [115]. Two types of the stacks were sputtered: substrate/Ta/MgO/CoFeB/Ta and substrate/Ta/CoFeB/MgO/Ta. For the first case, semi-crystalline state of CoFeB layer was found, for the second one, amorphous structure of CoFeB was present. Such result shows the other way to manipulate nucleation and movement of skyrmions. Introduction of additional layers between Ta and CoFeB has sufficient influence on DMI as well. It was shown that there is clear dependence between DMI constant and thickness of IrMn in case of its usage as an additional intermediate layer [116]. Recently, the creation of an individual stable skyrmions at RT and zero-field in films with AFM IrMn intermediate layer was shown in Ref. [117]. Moreover, the movement of skyrmions was induced by SOT effect using current pulses. This work gives a new opportunity to handle skyrmions. The use of AFM layers has several sufficient advantages: zero net magnetization, tuneable antiferromagnetic order, tuneable SOT strength, large exchange bias. Theoretically, all of these allow the creation of easy-tuneable, stable at RT, zero-field skyrmions. However, there is still a limited experimental demonstration and it has to be done during next couple of years.

In summary, CoFeB is a very promising material for any skyrmion application, in particular spintronic racetrack memory. CoFeB-based skyrmions show high stability at RT due to strong interfacial DMI. Several elements can be used as heavy metals: Pt, W, Ta. As shown above, DMI strongly depends on many parameters like deposition conditions, post-heat treatment parameters, types of alloying elements and substrates, *etc.* Other important issue besides DMI is the pinning of skyrmions, which directly influences the velocity of moving skyrmions along material. The pinning of skyrmions is not enough investigated and it directly depends on the crystal imperfections and defects, like grain boundaries. Besides, investigations will be directed to skyrmion size reduction with keeping high stability at RT and zero-field at the same time. Reduction of skyrmion size directly influences the memory density. The use of CoFeB films in combination with AFMs is also very promising approach and may be used in future manufacturing.

3.3. Platinum/Cobalt Multilayers for Skyrmion Memory Application

Pt/Co multilayers are in great demand regarding different memory and spintronic applications [124–126]. Recently possible skyrmion nucleation was discovered in Pt/Co ultrathin films [127, 128]. Boule *et al.* [118] investigated Néel-type skyrmions nucleation in Pt/Co/MgO stacks. The RT and zero-field skyrmions creation was demonstrated in Ref. [118]. Due to low DMI in ultrathin films, the use of multilayers seems to be more promising approach, as high amount of interfaces between FMs and SOC metals induces high net DMI inside [129, 130]. As a result, stacking of roughly 20 Co/Pt layers allows obtaining highly stable RT and zero-field skyrmions [122]. Introduction of an additional SOC metal to the Co/Pt system, for example, Ir or Ta, is an efficient way to increase the number of SOC–FM interfaces and DMI, respectively [121, 122]. Currently, a system of multiple layers of Ir/Fe/Co/Pt is the most promising films for skyrmion non-volatile memory applications [119–123].

4. Conclusions

The major state-of-the-art magnetic memory technologies were reported, and materials science aspects of the technologies were reviewed in this article. All STT-MRAM, AFM memory, and skyrmion racetrack memory could be used as the primary memory in desktops and laptops in the near future. Compared to other existing volatile (such as dynamic random access memory (DRAM)) or non-volatile (such as flash memory or phase-change memory) technologies, the magnetic memory technologies discussed here combine non-volatility, fast writing time, ultra-high density, and high endurance at the same time, making highly promising for future data storage applications.

Acknowledgements. This work was supported by the NATO SPS programme in the framework of the Multi-Year Project ‘Spintronic Devices for Microwave Detection and Energy Harvesting Applications’ (G5792) and by Ministry of Education and Science of Ukraine (Project Reg. No. 0119U001483).

REFERENCES

1. D. Edelstein, M. Rizzolo, D. Sil, A. Dutta, J. DeBrosse, M. Wordeman, A. Arceo, I.C. Chu, J. Demarest, E.R.J. Edwards, E.R. Evarts, J. Fullam, A. Gasasira, G. Hu, M. Iwatake, R. Johnson, V. Katragadda, T. Levin, J. Li, Y. Liu, C. Long, T. Maffitt, S. McDermott, S. Mehta, V. Mehta, D. Metzler, J. Morillo, Y. Nakamura, S. Nguyen, P. Nieves, V. Pai, R. Patlolla, R. Pujari, R. Southwick, T. Standaert, O. van der Straten, H. Wu, C.-C. Yang, D. Houssameddine, J.M. Slaughter, and D.C. Worledge, A 14 nm Embedded STT-MRAM CMOS Technology, *Proc. 2020 IEEE International Electron Devices Meeting (IEDM) (December 12–18, 2020)*; <https://www.ieee-iedm.org/iedm-archive>

2. J.C. Slonczewski, *J. Magn. Magn. Mater.*, **159**, Nos. 1–2: L1 (1996);
[https://doi.org/10.1016/0304-8853\(96\)00062-5](https://doi.org/10.1016/0304-8853(96)00062-5)
3. L. Berger, *Phys. Rev. B*, **54**, No. 13: 9353 (1996);
<https://doi.org/10.1103/PhysRevB.54.9353>
4. L. Zhu, S. Nie, K. Meng, D. Pan, J. Zhao, and H. Zheng, *Adv. Mater.*, **24**, No. 33: 4547 (2012);
<https://doi.org/10.1002/adma.201200805>
5. J.H. Park, Y.K. Hong, S. Bae, J.J. Lee, J. Jalli, G.S. Abo, and J.G. Lee, *J. Appl. Phys.*, **107**, No. 9: 09A731 (2010);
<https://doi.org/10.1063/1.3337640>
6. S. Ikeda, K. Miura, H. Yamamoto, K. Mizunuma, H.D. Gan, M. Endo, and H. Ohno, *Nature Mater.*, **9**, No. 9: 721 (2010);
<https://doi.org/10.1038/nmat2804>
7. S.J. Yun, S.H. Lim, and S.R. Lee, *Appl. Phys. Lett.*, **106**, No. 13, 132401 (2015);
<https://doi.org/10.1063/1.4916731>
8. J. Cao, J. Kanak, T. Stobiecki, P. Wisniewski, and P.P. Freitas, **45**, No. 10: 3464 (2009);
<https://doi.org/10.1109/TMAG.2009.2025382>
9. K. Okamoto, Y. Fuji, Y. Higashi, S. Kaji, T. Nagata, S. Baba, and M. Hara, *IEEE Transactions on Magnetics*, **54**, No. 11: 1 (2018);
<https://doi.org/10.1109/TMAG.2018.2835842>
10. T. Liu, Y. Zhang, J.W. Cai, and H.Y. Pan, *Sci. Rep.*, **4**: 5895 (2014);
<https://doi.org/10.1038/srep05895>
11. P. Khalili Amiri, Z.M. Zeng, J. Langer, H. Zhao, G. Rowlands, Y.J. Chen, and Y. Huai, *Appl. Phys. Lett.*, **98**, No. 11: 112507 (2011);
<https://doi.org/10.1063/1.3567780>
12. Y. Zhang, W. Zhao, Y. Lakys, J.O. Klein, J.V. Kim, D. Ravelosona, and C. Chappert, *IEEE Transactions on Electron Devices*, **59**, No. 3: 819 (2012);
<https://doi.org/10.1109/TED.2011.2178416>
13. V.B. Naik, H. Meng, and R. Shbiaa, *AIP Advances*, **2**, No. 4: 042182 (2012);
<https://doi.org/10.1063/1.4771996>
14. T. Ogasawara, M. Oogane, M. Al-Mahdawi, M. Tsunoda, and Y. Ando, *Sci. Rep.*, **9**: 1 (2019);
<https://doi.org/10.1038/s41598-019-53439-0>
15. Y.J. Chang, A. Canizo-Cabrera, V. Garcia-Vazquez, Y.H. Chang, and T.H. Wu, *J. Appl. Phys.*, **114**, No. 18: 184303 (2013);
<https://doi.org/10.1063/1.4829915>
16. H. Sato, M. Yamanouchi, S. Ikeda, S. Fukami, F. Matsukura, and H. Ohno, *Appl. Phys. Lett.*, **101**, No. 2: 022414 (2012);
<https://doi.org/10.1063/1.4736727>
17. F.T. Yuan, Y.H. Lin, J.K. Mei, J.H. Hsu, and P.C. Kuo, *J. Appl. Phys.*, **111**, No. 7: 07C111 (2012);
<https://doi.org/10.1063/1.3673408>
18. C.W. Cheng, W. Feng, G. Chern, C.M. Lee, and T.H. Wu, *J. Appl. Phys.*, **110**, No. 3: 033916 (2011);
<https://doi.org/10.1063/1.3621353>
19. T. Liu, J.W. Cai, and L. Sun, *AIP Advances*, **2**, No. 3: 032151 (2012);
<https://doi.org/10.1063/1.4748337>
20. W. Skowroński, T. Nozaki, D.D. Lam, Y. Shiota, K. Yakushiji, H. Kubota, and Y. Suzuki, *Phys. Rev. B*, **91**, No. 8: 184410 (2015);
<https://doi.org/10.1103/PhysRevB.91.184410>

21. C. Bilzer, T. Devolder, J.V. Kim, G. Council, C. Chappert, S. Cardoso, and P.P. Freitas, *J. Appl. Phys.*, **100**, No. 5: 053903 (2006);
<https://doi.org/10.1063/1.2337165>
22. C.L. Wang, S.H. Huang, C.H. Lai, W.C. Chen, S.Y. Yang, K.H. Shen, and H.Y. Bor, *J. Phys. D: Appl. Phys.*, **42**, 11: 115006 (2009);
<https://doi.org/10.1088/0022-3727/42/11/115006>
23. D. S. Wang, S.Y. Lai, T.Y. Lin, C.W. Chien, D. Ellsworth, L.W. Wang, and C.H. Lai, *Appl. Phys. Lett.*, **104**, No. 14: 142402 (2014);
<https://doi.org/10.1063/1.4870770>
24. A. Natarajarathinam, Z.R. Tadisina, T. Mewes, S. Watts, E. Chen, and S. Gupta, *J. Appl. Phys.*, **112**, No. 5: 053909 (2012);
<https://doi.org/10.1063/1.4749412>
25. S. Chen, M. Tang, Z. Zhang, B. Ma, S.T. Lou, and Q.Y. Jin, *Appl. Phys. Lett.*, **103**, No. 3: 032402 (2013);
<https://doi.org/10.1063/1.4813763>
26. A. Conca, E.T. Papaioannou, S. Klingler, J. Greser, T. Sebastian, B. Leven, and B. Hillebrands, *Appl. Phys. Lett.*, **104**, No. 18: 182407 (2014);
<https://doi.org/10.1063/1.4875927>
27. D. Jhahhria, D.K. Pandya, and S. Chaudhary, *AIP Conf. Proc.*, **1953**, No. 1: 120034 (2018);
<https://doi.org/10.1063/1.5033099>
28. K. Kamino, T. Kawaguchi, and M. Nagakura, *IEEE Transactions on Magnetics*, **2**: 506 (1966);
<https://doi.org/10.1109/TMAG.1966.1065887>
29. M. Oogane, K. Watanabe, H. Saruyama, M. Hosoda, P. Shahnaz, Y. Kurimotom, and Y. M. Ando, *Jpn. J. Appl. Phys.*, **56**: 0802A2 (2017);
<https://doi.org/10.7567/JJAP.56.0802A2>
30. S.H. Nie, L.J. Zhu, J. Lu, D. Pan, H.L. Wang, X.Z. Yu, J.X. Xiao, and J.H. Zhao, *Appl. Phys. Lett.*, **102**, No. 15: 152405 (2013);
<https://doi.org/10.1063/1.4801932>
31. T. Sato, T. Ohsuna, and Y. Kaneko, *J. Appl. Phys.*, **120**: 243903 (2016);
<https://doi.org/10.1063/1.4972972>
32. G.A. Fischer and M. L. Rudee, *J. Magn. Magn. Mater.*, **213**: 335 (2000);
[https://doi.org/10.1016/S0304-8853\(00\)00007-X](https://doi.org/10.1016/S0304-8853(00)00007-X)
33. S.L. Zhu, S. Nie, K. Meng, D. Pan, J. Zhao, H. Zheng, *Adv. Mater.*, **24**: 4547 (2012);
<https://doi.org/10.1002/adma.201200805>
34. S. Mao, J. Lu, X. Zhao, X. Wang, D. Wei, J. Liu, and J. Zhao, *Sci. Rep.*, **7**: 43064 (2017);
<https://doi.org/10.1038/srep43064>
35. A. Ono, K.Z. Suzuki, R. Ranjbar, A. Sugihara, and S. Mizukami, *Appl. Phys. Express*, **10**: 023005 (2017);
<https://doi.org/10.7567/APEX.10.023005>
36. K. Sato, Y. Takahashi, H. Makuta, T. Shima, and M. Doi, *J. Magn. Soc. Jpn.*, **2**: 48 (2018);
<https://doi.org/10.20819/msjtsj.18TR211>
37. Y. Takahashi, H. Makuta, T. Shima, and M. Doi, *Trans. Magn. Soc. Jpn.*, **1**: 30 (2017);
<https://doi.org/10.20819/msjtsj.17TR107>
38. X. Zhang, L.L. Tao, J. Zhang, S. H. Liang, L. Jiang, and X. F. Han, *Appl. Phys. Lett.*, **110**: 252403 (2017);
<https://doi.org/10.1063/1.4986449>

39. H. Saruyama, M. Oogane, Y. Kurimoto, H. Naganuma, and Y. Ando, *Jpn. J. Appl. Phys.*, **52**: 063003 (2013);
<https://doi.org/10.7567/JJAP.52.063003>
40. S. Mao, J. Lu, H. Wang, X. Zhao, D. Wei, and J. Zhao, *J. Phys. D: Appl. Phys.*, **52**: 405002 (2019);
<https://doi.org/10.1088/1361-6463/ab300a>
41. T. Kubota, Q. Ma, S. Mizukami, X. Zhang, H. Naganuma, M. Oogane, Y. Ando, and T. Miyazaki, *Appl. Phys. Express*, **5**: 043003 (2012);
<https://doi.org/10.1143/APEX.5.043003>
42. K.Z. Suzuki, R. Ranjbar, J. Okabayashi, Y. Miura, A. Sugihara, H. Tsuchiura, and S. Mizukami, *Sci. Rep.*, **6**: 30249 (2016);
<https://doi.org/10.1038/srep30249>
43. Q. L. Ma, T. Kubota, S. Mizukami, X. M. Zhang, H. Naganuma, M. Oogane, Y. Ando, and T. Miyazaki, *Appl. Phys. Lett.*, **101**: 032402 (2012);
<https://doi.org/10.1063/1.4737000>
44. S. Mizukami, A. Sugihara, S. Iihama, Y. Sasaki, K. Z. Suzuki, and T. Miyazaki, *Appl. Phys. Lett.*, **108**: 012404 (2016);
<https://doi.org/10.1063/1.4939447>
45. J.H. Park, Y.K. Hong, S. Bae, J.J. Lee, J. Jalli, G.S. Abo, N. Neveu, S.G. Kim, C.J. Choi, and J.G. Lee, *J. Appl. Phys.*, **107**: 09A731 (2010);
<https://doi.org/10.1063/1.3337640>
46. K. Watanabe, M. Oogane, and Y. Ando, *Jpn. J. Appl. Phys.*, **56**: 0802B1 (2017);
<https://doi.org/10.7567/JJAP.56.0802B1>
47. L. Hou-Fang, S.S. Ali, and H. Xiu-Feng, *Chinese Phys. B*, **23**: 077501 (2014);
<https://doi.org/10.1088/1674-1056/23/7/077501>
48. K.Z. Suzuki, Y. Miura, R. Ranjbar, L. Bainsla, A. Ono, Y.Sasaki, and S. Mizukami, *Appl. Phys. Lett.*, **112**: 062402 (2018);
<https://doi.org/10.1063/1.5002616>
49. N. Inami, G. Kim, T. Hiratuka, H. Naganuma, M. Oogane and Y. Ando, *J. Phys.: Conf. Ser.*, **200**: 052008 (2010);
<https://doi.org/10.1088/1742-6596/200/5/052008>
50. G. Yang, D.L. Li, S.G. Wang, Q.L. Ma, S.H. Liang, H.X. Wei, X.F. Han, T. Hesjedal, R.C.C. Ward, A. Kohn, A. Elkayam, N. Tal, and X.-G. Zhang, *J. Appl. Phys.*, **117**: 083904 (2015);
<https://doi.org/10.1063/1.4913265>
51. S. Ikeda, K. Miura, H. Yamamoto, K. Mizunuma, H.D. Gan, M. Endo, S. Kanai, J. Hayakawa, F. Matsukura, and H. Ohno, *Nat. Mater.*, **9**: 721 (2010);
<https://doi.org/10.1038/nmat2804>
52. S. Iihama, A. Sakuma, H. Naganuma, M. Oogane, S. Mizukami, and Y. Ando, *Phys. Rev. B*, **94**: 174425 (2016);
<https://doi.org/10.1103/PhysRevB.94.174425>
53. S. Iihama, M. Khan, H. Naganuma, M. Oogane, T. Miyazaki, S. Mizukami, and Y. Ando, *J. Magn. Soc. Jpn.*, **39**: 57 (2015);
<https://doi.org/10.3379/msjmag.1501R004>
54. T. Bae, J. Ko, S. Lee, J. Cha, and J. Hong, *Jpn. J. Appl. Phys.*, **55**, No. 1: 013001 (2015);
<https://doi.org/10.7567/JJAP.55.013001>
55. D. Zhang, D. Huang, R.J. Wu, D. Lattery, J. Liu, X. Wang, and X. Wang, *Appl. Phys. Lett.*, **117**, No. 8: 082405 (2020);
<https://doi.org/10.1063/5.0016100>

56. D.L. Zhang, K.B. Schliep, R.J. Wu, P. Quarterman, D. Reifsnnyder Hickey, Y. Lv, and J.P. Wang, *Appl. Phys. Lett.*, **112**, No. 15: 152401 (2018); <https://doi.org/10.1063/1.5019193>
57. F. Máca, J. Kudrnovský, P. Baláž, V. Drchal, K. Carva, and I. Turek, *J. Magn. Magn. Mater.*, **474**: 467 (2019); <https://doi.org/10.1016/j.jmmm.2018.10.145>
58. K. Uhlířová, E. Duverger-Nédellec, R.H. Colman, J. Volný, B. Vondráčková, and K. Carva, *J. Alloys Compd.*, **771**: 680 (2019); <https://doi.org/10.1016/j.jallcom.2018.08.199>
59. X. Marti, I. Fina, C. Frontera, J. Liu, P. Wadley, Q. He, and J. Kuneš, *Nature Mater.*, **13**, No. 4: 367 (2014); <https://doi.org/10.1038/nmat3861>
60. J. Železný, P. Wadley, K. Olejník, A. Hoffmann, and H. Ohno, *Nature Phys.*, **14**, No. 3: 220 (2018); <https://doi.org/10.1038/s41567-018-0062-7>
61. H. Kumar, D.R. Cornejo, S.L. Morelhao, S. Kycia, I.M. Montellano, N.R. Álvarez, and A. Butera, *J. Appl. Phys.*, **124**, No. 8: 085306 (2018); <https://doi.org/10.1063/1.5020160>
62. Z. Liu, Z. Feng, H. Yan, X. Wang, X. Zhou, P. Qin, and C. Jiang, *Adv. Electron. Mater.*, **5**, No. 7: 1900176 (2019).
63. T. Kampfrath, A. Sell, G. Klatt, A. Pashkin, S. Mährlein, T. Dekorsy, and R. Huber, *Nature Photonics*, **5**, No. 1: 31 (2011); <https://doi.org/10.1038/nphoton.2010.259>
64. K. Olejník, T. Seifert, Z. Kašpar, V. Novák, P. Wadley, R.P. Campion, and J. Sinova, *Science Adv.*, **4**, No. 3: eaar3566 (2018); <https://doi.org/10.1126/sciadv.aar3566>
65. P. Wadley, B. Howells, J. Železný, C. Andrews, V. Hills, R.P. Campion, and S.Y. Martin, *Science*, **351**, No. 6273: 587 (2016); <https://doi.org/10.1126/science.aab1031>
66. S.Y. Bodnar, L. Jbmejkal, I. Turek, T. Jungwirth, O. Gomonay, J. Sinova, and M. Jourdan, *Nature Commun.*, **9**, No. 1: 1 (2018); https://doi.org/10.1007/978-3-319-97334-0_9
67. H. Yan, Z. Feng, S. Shang, X. Wang, Z. Hu, J. Wang, and W. Lu, *Nature Nanotechnol.*, **14**: 131 (2019); <https://doi.org/10.1038/s41565-018-0339-0>
68. A. Ceballos, Z. Chen, O. Schneider, C. Bordel, L.W. Wang, and F. Hellman, *Appl. Phys. Lett.*, **111**, No. 17: 172401 (2017); <https://doi.org/10.1063/1.4997901>
69. I. Suzuki, T. Koike, M. Itoh, T. Taniyama, and T. Sato, *J. Appl. Phys.*, **105**, No. 7: 07E501 (2009); <https://doi.org/10.1063/1.3054386>
70. A. Ceballos, Z. Chen, O. Schneider, C. Bordel, L.W. Wang, and F. Hellman, *Appl. Phys. Lett.*, **111**, No. 17: 172401 (2017); <https://doi.org/10.1063/1.4997901>
71. R.F. Need, J. Lauzier, L. Sutton, B.J. Kirby, and J. De La Venta, *APL Materials*, **7**, No. 10: 101115 (2019); <https://doi.org/10.1063/1.5118893>
72. P. Wadley, V. Novák, R.P. Campion, C. Rinaldi, X. Martí, H. Reichlová, and D. Khalayavin, *Nature Commun.*, **4**, No. 1: 1 (2013); <https://doi.org/10.1038/ncomms3322>

73. K.A. Omari, L.X. Barton, O. Amin, R.P. Champion, A.W. Rushforth, A.J. Kent, and K.W. Edmonds, *J. Appl. Phys.*, **127**, No. 19: 193906 (2020);
<https://doi.org/10.1063/5.0006183>
74. F. Máca, J. Maňek, O. Stelmakhovych, X. Martí, H. Reichlová, K. Uhlířová, and T. Jungwirth, *J. Magn. Magn. Mater.*, **324**, No. 8: 1606 (2012);
<https://doi.org/10.1016/j.jmmm.2011.12.017>
75. T. Matalla-Wagner, M.F. Rath, D. Graulich, J.M. Schmalhorst, G. Reiss, and M. Meinert, *Phys. Rev. Appl.*, **12**, No. 6: 064003 (2019);
<https://doi.org/10.1103/PhysRevApplied.12.064003>
76. P. Wadley, V. Hills, M.R. Shahedkhah, K.W. Edmonds, R.P. Champion, V. Novák, and P. Nemeč, *Sci. Rep.*, **5**: 17079 (2015);
<https://doi.org/10.1038/srep17079>
77. H.C. Wu, Z.M. Liao, R.S. Sofin, G. Feng, X.M. Ma, A.B. Shick, and I.V. Shvets, *Adv. Mater.*, **24**, No. 47: 6374 (2012);
<https://doi.org/10.1002/adma.201202273>
78. M. Meinert, D. Graulich, and T. Matalla-Wagner, *Phys. Rev. Appl.*, **9**, No. 6: 064040 (2018);
<https://doi.org/10.1103/PhysRevApplied.9.064040>
79. S. Khmelevskiy and P. Mohn, *Appl. Phys. Lett.*, **93**, No. 16: 162503 (2008);
<https://doi.org/10.1063/1.3003878>
80. V.M.T.S. Barthem, C.V. Colin, H. Mayaffre, M.H. Julien, and D. Givord, *Nature Commun.*, **4**, No. 1: 1 (2013);
<https://doi.org/10.1038/ncomms3892>
81. M. Jourdan, H. Bräuning, A. Sapozhnik, H.J. Elmers, H. Zabel, and M. Kläui, *J. Phys. D: Appl. Phys.*, **48**, No. 38: 385001 (2015);
<https://doi.org/10.1088/0022-3727/48/38/385001>
82. A.A. Sapozhnik, M. Filianina, S.Y. Bodnar, A. Lamirand, M.A. Mawass, Y. Skourski, and M. Jourdan, *Phys. Rev. B*, **97**, No. 13: 134429 (2018);
<https://doi.org/10.1103/PhysRevB.97.134429>
83. S.Y. Bodnar, M. Filianina, S.P. Bommanaboyena, T. Forrest, F. Maccherozzi, A.A. Sapozhnik, and M. Jourdan, *Phys. Rev. B*, **99**, No. 14: 140409 (2019);
<https://doi.org/10.1103/PhysRevB.99.140409>
84. D. Zhu, W. Kang, S. Li, Y. Huang, X. Zhang, Y. Zhou, and W. Zhao, *IEEE Transactions on Electron Devices*, **65**, No. 1: 87 (2017);
<https://doi.org/10.1109/TED.2017.2769672>
85. K. Wang, L. Qian, S.C. Ying, G. Xiao, and X. Wu, *Nanoscale*, **11**, No. 14: 6952 (2019);
<https://doi.org/10.1039/C9NR00909D>
86. J. Sampaio, V. Cros, S. Rohart, A. Thiaville, and A. Fert, *Nature Nanotechnol.*, **8**, No. 11: 839 (2013);
<https://doi.org/10.1038/nnano.2013.210>
87. S. Rohart and A. Thiaville, *Phys. Rev. B*, **88**, No. 18: 184422 (2013);
<https://doi.org/10.1103/PhysRevB.88.184422>
88. P. Ferriani, K. Von Bergmann, E.Y. Vedmedenko, S. Heinze, M. Bode, M. Heide, and R. Wiesendanger, *Phys. Rev. Lett.*, **101**, No. 2: 027201 (2008);
<https://doi.org/10.1103/PhysRevLett.101.027201>
89. M. Bode, M. Heide, K. Von Bergmann, P. Ferriani, S. Heinze, G. Bihlmayer, and R. Wiesendanger, *Nature*, **447**, No. 7141: 190 (2007);
<https://doi.org/10.1038/nature05802>
90. S. Mühlbauer, B. Binz, F. Jonietz, C. Pfleiderer, A. Rosch, A. Neubauer, and P. Böni, *Science*, **323**, No. 5916: 915 (2009);
<https://doi.org/10.1126/science.1166767>

91. S.X. Huang and C.L. Chien, *Phys. Rev. Lett.*, **108**, No. 26: 267201 (2012);
<https://doi.org/10.1103/PhysRevLett.108.267201>
92. F. Albert, R. Nicolas, and C. Vincent, *Nature Rev. Mater.*, **2**: 17031 (2017);
<https://doi.org/10.1038/natrevmats.2017.31>
93. W. Münzer, A. Neubauer, T. Adams, S. Mühlbauer, C. Franz, F. Jonietz, and A. Rosch, *Phys. Rev. B*, **81**, No. 4: 041203 (2010);
<https://doi.org/10.1103/PhysRevB.81.041203>
94. X.Z. Yu, Y. Onose, N. Kanazawa, J.H. Park, J.H. Han, Y. Matsui, and Y. Tokura, *Nature*, **465**, No. 7300: 901 (2010);
<https://doi.org/10.1038/nature09124>
95. S. Heinze, K. Von Bergmann, M. Menzel, J. Brede, A. Kubetzka, R. Wiesendanger, and S. Blügel, *Nature Phys.*, **7**, No. 9: 713 (2011);
<https://doi.org/10.1038/nphys2045>
96. N. Romming, C. Hanneken, M. Menzel, J.E. Bickel, B. Wolter, K. von Bergmann, and R. Wiesendanger, *Science*, **341**, No. 6146: 636 (2013);
<https://doi.org/10.1126/science.1240573>
97. W. Legrand, D. Maccariello, F. Ajejas, S. Collin, A. Vecchiola, K. Bouzehouane, and A. Fert, *Nature Mater.*, **19**, No. 1: 34 (2020);
<https://doi.org/10.1038/s41563-019-0468-3>
98. W. Legrand, D. Maccariello, N. Reyren, K. Garcia, C. Moutafis, C. Moreau-Luchaire, and A. Fert, *Nano Lett.*, **17**, No. 4: 2703 (2017);
<https://doi.org/10.1021/acs.nanolett.7b00649>
99. S.A. Montoya, R. Tolley, I. Gilbert, S.G. Je, M.Y. Im, and E.E. Fullerton, *Phys. Rev. B*, **98**, No. 10: 104432 (2018);
<https://doi.org/10.1103/PhysRevB.98.104432>
100. R. Wiesendanger, *Nature Rev. Mater.*, **1**: 16044 (2016);
<https://doi.org/10.1038/natrevmats.2016.44>
101. C. Hanneken, F. Otte, A. Kubetzka, B. Dupé, N. Romming, K. Von Bergmann, and S. Heinze, *Nature Nanotechnol.*, **10**, No. 12: 1039 (2015);
<https://doi.org/10.1038/nnano.2015.218>
102. D.M. Crum, M. Bouhassoune, J. Bouaziz, B. Schweflinghaus, S. Blügel, and S. Lounis, *Nature Commun.*, **6**: 8541 (2015);
<https://doi.org/10.1038/ncomms9541>
103. K. Everschor, M. Garst, B. Binz, F. Jonietz, S. Mühlbauer, C. Pfleiderer, and A. Rosch, *Phys. Rev. B*, **86**, No. 5: 054432 (2012);
<https://doi.org/10.1103/PhysRevB.86.054432>
104. J. Iwasaki, M. Mochizuki, and N. Nagaosa, *Nature Commun.*, **4**: 1463 (2013);
<https://doi.org/10.1038/ncomms2442>
105. J. Iwasaki, M. Mochizuki, and N. Nagaosa, *Nature Nanotechnol.*, **8**, No. 10: 742 (2013);
<https://doi.org/10.1038/nnano.2013.176>
106. J. Sampaio, V. Cros, S. Rohart, A. Thiaville, and A. Fert, *Nature Nanotechnol.*, **8**, No. 11: 839 (2013);
<https://doi.org/10.1038/nnano.2013.210>
107. R. Tomasello, E. Martinez, R. Zivieri, L. Torres, M. Carpentieri, and G. Finocchio, *Sci. Rep.*, **4**: 6784 (2014);
<https://doi.org/10.1038/srep06784>
108. S. Woo, K. Litzius, B. Krüger, M.-Y. Im, L. Caretta, K. Richter, M. Mann, A. Krone, R.M. Reeve, M. Weigand, P. Agrawal, I. Lemesch, M.-A. Mawass, P. Fischer, M. Kläui, and G.S. D. Beach, *Nature Mater.*, **15**, No. 5: 501 (2016);
<https://doi.org/10.1038/nmat4593>

109. D. Stosic, J. Mulkers, B. Van Waeyenberge, T.B. Ludermit, and M.V. Milošević, *Phys. Rev. B*, **95**, No. 21: 214418 (2017);
<https://doi.org/10.1103/PhysRevB.95.214418>
110. D. Stosic, T.B. Ludermit, and M.V. Milošević, *Phys. Rev. B*, **96**, No. 21: 214403 (2017);
<https://doi.org/10.1103/PhysRevB.96.214403>
111. K. Di, V.L. Zhang, H.S. Lim, S.C. Ng, M.H. Kuok, X. Qiu, and H. Yang, *Appl. Phys. Lett.*, **106**, No. 5: 052403 (2015);
<https://doi.org/10.1063/1.4907173>
112. S. Jaiswal, K. Litzius, I. Lemesh, F. Büttner, S. Finizio, J. Raabe, M. Weigand, K. Lee, J. Langer, B. Ocker, G. Jakob, G.S.D. Beach, and M. Kläui, *Appl. Phys. Lett.*, **111**, No. 2: 022409 (2017);
<https://doi.org/10.1063/1.4991360>
113. R.A. Khan, P.M. Shepley, A. Hrabec, A.W.J. Wells, B. Ocker, C.H. Marrows, and T.A. Moore, *Appl. Phys. Lett.*, **109**, No. 13: 132404 (2016)
<https://doi.org/10.1063/1.4963731>
114. Z. Qin, C. Jin, H. Xie, X. Li, Y. Wang, J. Cao, and Q. Liu, *J. Phys. D: Appl. Phys.*, **51**, No. 42: 425001 (2018);
<https://doi.org/10.1088/1361-6463/aadd59>
115. H. Yin, X. Zheng, J. Wang, Y. Zhou, B. Kuerbanjiang, G. Li, X. Lu, Y. Wang, J. Wu, V.K. Lazarov, R.F.L. Evans, R. W. Chantre, J. Cai, B. Liu, H. Meng, and Y. Xu, arXiv:2006.02864 (2020).
116. C. He, S.A. Razavi, G. Yu, X. Ma, H. Wu, Q. Shao, K.L. Wong, S. Shen, Y. Zhao, Y. Pei, Q. Chen, X. Li, S. Wang, and K.L. Wang, *Appl. Phys. Lett.*, **116**, No. 24: 242407 (2020);
<https://doi.org/10.1063/5.0006138>
117. G. Yu, A. Jenkins, X. Ma, S.A. Razav, C. He, G. Yin, Q. Shao, Q.L. He, H. Wu, W. Li, W. Jiang, X. Han, X. Li, A.C. Bleszynski Jayich, P.K. Amiri, and K.L. Wang, *Nano Lett.*, **18**, No. 2: 980 (2018);
<https://doi.org/10.1021/acs.nanolett.7b04400>
118. O. Boulle, J. Vogel, H. Yang, S. Pizzini, D. de Souza Chaves, A. Locatelli, T.O. Menteş, A. Sala, L.D. Buda-Prejbeanu, O. Klein, M. Belmeguenai, Y. Rous-signé, A. Stashkevich, S.M. Chérif, L. Aballe, M. Foerster, M. Chshiev, S. Auf-fret, I.M. Miron, and G. Gaudin, *Nature Nanotechnol.*, **11**, No. 5: 449 (2016);
<https://doi.org/10.1038/nnano.2015.315>
119. A. Yagil, A. Almoalem, A. Soumyanarayanan, A.K. Tan, M. Raju, C. Panago-poulos, and O.M. Auslaender, *Appl. Phys. Lett.*, **112**, No. 19: 192403 (2018);
<https://doi.org/10.1063/1.5027602>
120. A. Soumyanarayanan, M. Raju, A.L. Gonzalez Oyarce, A.K.C. Tan, M. Im, A.P. Petrović, P. Ho, K.H. Khoo, M. Tran, C.K. Gan, F. Ernult, and C. Pana-gopoulo, *Nature Mater.*, **16**, No. 9: 898 (2017);
<https://doi.org/10.1038/nmat4934>
121. M. Raju, A. Yagil, A. Soumyanarayanan, A.K. Tan, A. Almoalem, F. Ma, and C. Panagopoulos, *Nature Commun.*, **10**: 696 (2019);
<https://doi.org/10.1038/s41467-018-08041-9>
122. N.K. Duong, M. Raju, A.P. Petrović, R. Tomasello, G. Finocchio, and C. Pana-gopoulos, *Appl. Phys. Lett.*, **114**, No. 7: 072401 (2019);
<https://doi.org/10.1063/1.5080713>
123. D. Maccariello, W. Legrand, N. Reyren, K. Garcia, K. Bouzehouane, S. Collin, and A. Fert, *Nature Nanotechnol.*, **13**, No. 3: 233 (2018);
<https://doi.org/10.1038/s41565-017-0044-4>

124. J.-H. Park, C. Park, T. Jeong, M.T. Moneck, N.T. Nufer, and J.-G. Zhu, *J. Appl. Phys.*, **103**, No. 7: 07A917 (2008);
<https://doi.org/10.1063/1.2838754>
125. V. Baltz, A. Marty, B. Rodmacq, and B. Dieny, *Phys. Rev. B*, **75**, No. 1: 014406 (2007);
<https://doi.org/10.1103/PhysRevB.75.014406>
126. J. Sort, A. Popa, B. Rodmacq, and B. Dieny, *Phys. Rev. B*, **70**, No. 17: 174431 (2004);
<https://doi.org/10.1103/PhysRevB.70.174431>
127. R. Juge, S.-G. Je, D. de Souza Chaves, L.D. Buda-Prejbeanu, J. Peca-Garcia, J. Nath, I.M. Miron, K.G. Rana, L. Aballe, M. Foerster, F. Genuzio, T.O. Mentès, A. Locatelli, F. Maccherozzi, S.S. Dhesi, M. Belmeguenai, Y. Roussigné, S. Auffret, S. Pizzini, G. Gaudin, J. Vogel, and O. Boulle, *Phys. Rev. Appl.*, **12**, No. 4: 044007 (2019);
<https://doi.org/10.1103/PhysRevApplied.12.044007>
128. S. Rohart and A. Thiaville, *Phys. Rev. B*, **88**, 18: 184422 (2013);
<https://doi.org/10.1103/PhysRevB.88.184422>
129. S. Zhang, J. Zhang, Y. Wen, E.M. Chudnovsky, and X. Zhang, *Appl. Phys. Lett.*, **113**, No. 19: 192403 (2018);
<https://doi.org/10.1063/1.5053983>
130. M. He, L. Peng, Z. Zhu, G. Li, J. Cai, J. Li, H. Wei, L. Gu, S. Wang, T. Zhao, B. Shen, and Y. Zhang, *Appl. Phys. Lett.*, **111**, No. 20: 202403 (2017);
<https://doi.org/10.1063/1.5001322>

Received 10.03.2021;
in final version, 09.06.2021

А.Е. Гафаров¹, С.М. Волошко¹, А. Кайдатцис², І.А. Владимирський¹

¹ Кафедра фізики металів, Національний технічний університет України
«Київський політехнічний інститут імені Ігоря Сікорського»,
проспект Перемоги, 37, 03056 Київ, Україна

² Інститут нанотехнологій, Демокритос, Агія Параскеви Аттікис,
15310 Афіни, Греція

НАНОМАСШТАБНІ МАТЕРІАЛИ ДЛЯ СУЧАСНИХ ТЕХНОЛОГІЙ МАГНЕТНОГО ЗАПИСУ

В огляді висвітлено матеріалознавчі аспекти сучасних технологій магнетної пам'яті, такі як магнеторезистивна оперативна пам'ять із довільним доступом (MRAM), антиферомагнетна пам'ять і трекова скірміонна пам'ять. Зокрема, матеріали з великою перпендикулярною магнетною анізотропією, такі як стопи CoFeB, $L1_0$ -впорядковані стопи на основі Mn та Fe, розглянуто (розд. 1) стосовно застосування їх у технології магнеторезистивної оперативної пам'яті. Окрім того, розглянуто (розд. 2) дослідження антиферомагнетних стопів, таких як FeRh, CuMnAs, Mn_2Au . Нарешті, останній розділ (розд. 3) огляду стосується матеріалів, які можуть бути використані у трековій скірміонній пам'яті.

Ключові слова: МРОП, спінтроніка, магнетні матеріали, антиферомагнетики, скірміон.